Proceedings of the Institute of Acoustics

VARIABILITY IN MODELLED SONAR AND TARGET DEPTH DISTRIBUTIONS

Kristoffer Engedal Andreassen — Norwegian Defence Research Establishment (FFI), Kjeller, Norway

Karl Thomas Hjelmervik — University of South-Eastern Norway (USN), Horten, Norway

1 INTRODUCTION

Sonar performance depends heavily on the present environment, particularly the oceanography, bottom topography, bottom sediments, and surface wave conditions. Acoustic models provide insight on the impact of each environmental parameter. The impact is often heavily frequency-dependent, and for sonar systems in the low KHz-domain the most important factors are the sound speed profile (SSP), topography, and the surface wave conditions.

For sonar experiments, measurements of the sound speed, local wind speed measurements, and a topographic model are used as input to sonar performance models. A sonar operator or an algorithm may optimise the sonar parameters for the present conditions by first testing them in acoustic models[1]. The increasing availability of high-quality oceanographic data, e.g. climatology and ocean models[2], allow more refined methods that account for variability and uncertainty[3,4,5].

Consider a vessel equipped with a variable depth active sonar searching for a subsurface target surveying the surface with a passive sonar. The target wants to remain undetected by the surface vessel, while maximising its own ability to detect other vessels. For a given environment, the sonar performance depends heavily on the relative positions of target, source, and receivers[6]. In a previous work[7] we employed game theory to explore this optimisation problem. There we determined target and sonar depths using the Nash equilibrium[8] strategies for the two opponents. For a sample environment, such a method can be used to find best avoidance and detection depths for both parties. However, this approach fails to capture the environmental uncertainty and any further analysis is limited to a single environment, which may cause problems in terms of robustness.

This game theoretical method is what we aim to improve by introducing environmental variability, continuing to utilise the fast and environmentally configurable acoustic ray tracing model Lybin[9]. The resulting single Nash equilibrium target and sonar depths can then be aggregated into distributions representative for the present environment.

2 METHOD

The method proposed here expands upon previous work[7] by introducing spatially varying bottom depths and spatio-temporal variations in sound speed profiles (SSPs) and wind. To do this, we need to calculate a payoff matrix[10] which depends on the bearing θ and range r from the active sonar position and the current time t:

$$U(z, d; t, \theta, r) = (1 - U_A(z, d; t, \theta, r)) \cdot U_P(z; t, \theta, r). \tag{1}$$

The payoff is a product of the probability of avoiding active detection $(1 - U_A)$ and the probability of having passive surface coverage (U_P), which the underwater target seeks to maximise by selecting its depth z. Simultaneously, the active sonar agent seeks to minimise this payoff by selecting its variable sonar depth d (assuming here a co-located transmitter and receiver). For each tuple of (t, θ, r), this is optimally solved by finding the set of Nash equilibrium strategies. These strategies are guaranteed to exist if one allows for mixed-strategies[11], which are maps from our possible alternatives $(\mathcal{Z}, \mathcal{D})$ to probability simplexes $(\boldsymbol{R}^{\mathcal{Z}}, \boldsymbol{R}^{\mathcal{D}})$. Unlike pure strategies, which recommend only a single alternative, these can assign non-zero probabilities to several alternatives. For a two-player zero sum game defined by Eq. 1, these strategies can be efficiently found by formulating the problem as a linear program[10], which we implement via NashPy[12].

The bottleneck for modelling the variability present in an area is in running a suitable acoustic model for each (t, θ, r) in order to calculate both U_A and U_P. We propose to divide the relevant area into annular sector subareas, as shown in Fig. 1. The sectors' angular width is kept constant at $360°/B$, where B is the number of different bearings from the active sonar considered. The inner and outer ranges of each annular sector subarea are chosen such that the surface area of each subarea remains constant. Each bearing consists of R subareas defined by these ranges, making the total number of subareas $B \times R$. A 2D acoustic model can cover all R ranges and relevant target depths z in one run, but will need $B \times D$ runs to cover all bearings and the number of active sonar depths D.

In principle, the passive sonar performance in each subarea will also have environmental bearing and range dependence, as it will aim to detect an arbitrary noisy surface vessel with an unknown position. In order to simplify the number of acoustic model runs required to calculate U_P, we use constant bottom depths, wind and sound speed profiles for each subarea, sampled at the centroid of each subarea (marked with red stars in Fig. 1). The total number of acoustic model runs required for each active sonar position is therefore

$$T \times B \times (D + R), \tag{2}$$

where T is the number of different times samples t considered. For each (t, θ, r) we can then calculate the Nash equilibrium strategies and aggregate them into a single global distribution of strategies for both the active sonar and the target.

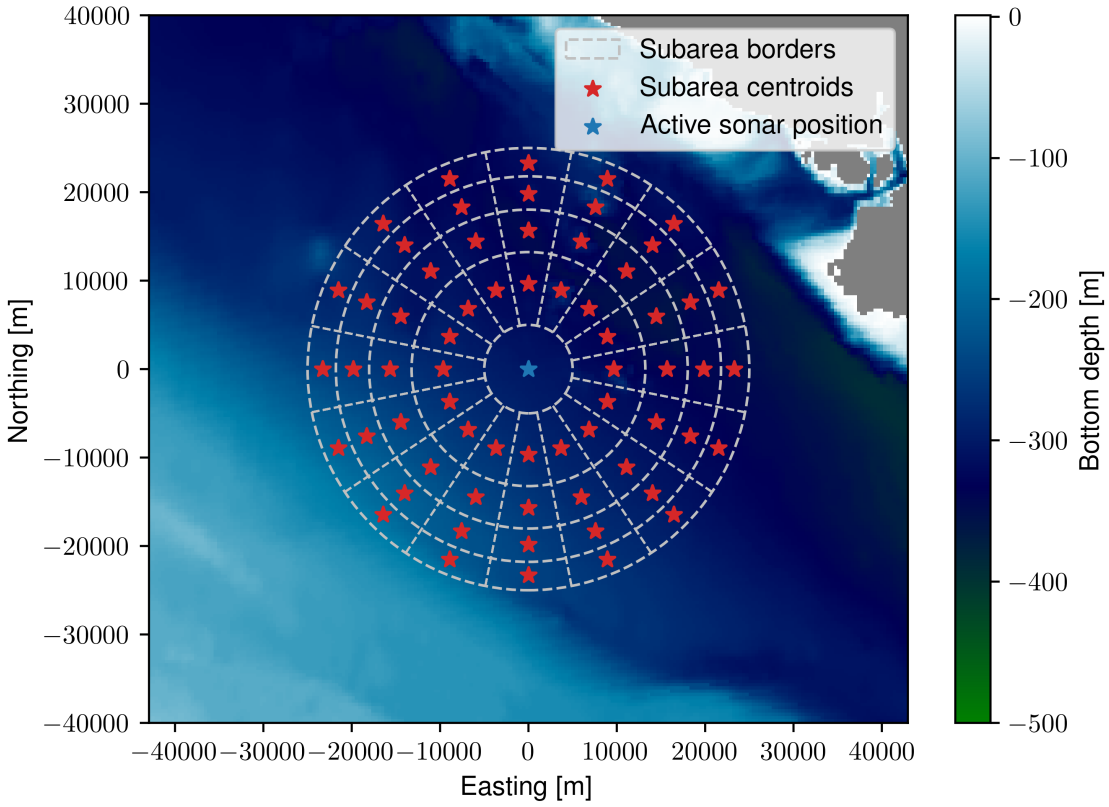

Figure 1: Bottom depths for the test area supplied by GEBCO[13], with subarea division and centroids for $B = 16$ ***and*** $R = 4$***.***

3 DATASET

We demonstrate the proposed method for a test area with notable variation in both bathymetry and oceanography. The global topographic model GEBCO[13], which has 15 arc-second resolution, is used to extract the required topographic profiles. Fig. 1 shows the topography of the area, consisting of upslopes which flank an approximately 300 m deep trench going North-West to South-East. The subareas start at 5 km range and end at 25 km, which means that targets outside that range are not optimised for.

The range-dependent sound speed profiles and wind profiles are taken from NorKyst800[2], which is the main ocean forecasting tool for Norwegian waters, with a spatial resolution of 800 m. Fig. 2 shows a sample of the sea surface temperature and wind speed in the selected area. The sea surface temperature shows signs of eddy currents and fronts, both of which may cause significant range-dependent acoustic propagation effects. The wind and SSP are sampled at 10 points along each bearing out to the max range of 25 km.

The times sampled from the model are from May 12th to 17th 2023, but we limit ourselves to the 5 hourly snapshots around midnight (22:00 to 02:00 UTC), making the number of time samples $T = 25$. A cloud of

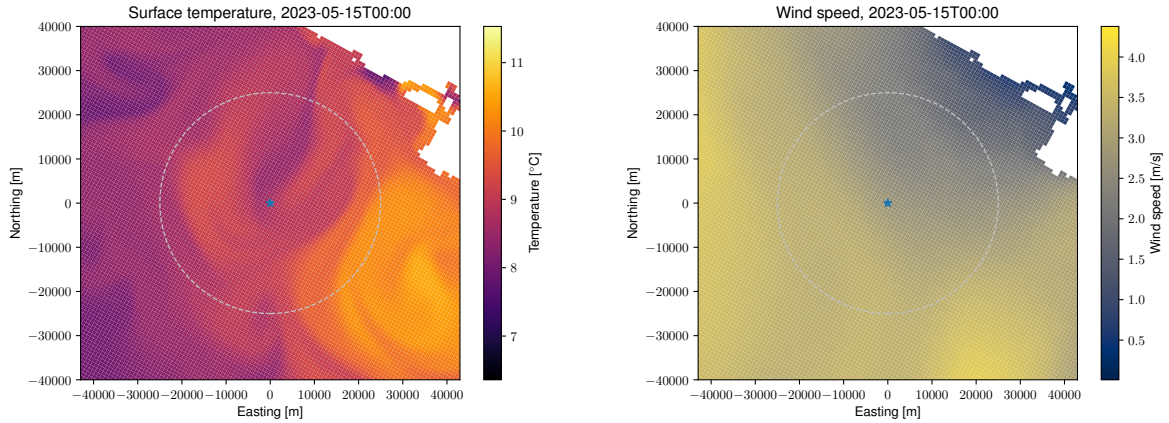

Figure 2: Sea surface temperature in °C (left) and surface wind speed (right) taken from the NorKyst800 model[2] output for 15th of May 2023, at 00:00 UTC. Active sonar position marked with blue star and max range with dashed circle.

sound speed profiles taken from the ocean model at those times is shown in Fig. 3. The profiles exhibit a typical late spring behaviour, showing a strong sound channel with a sound speed minimum varying between 25 m and 75 m depth.

4 RESULTS AND DISCUSSION

Applying the method in section 2 on the dataset in section 3, Fig. 3 shows the resulting sonar depth distribution for $B = 128$ and $R = 4$. The available sonar depths were bounded between 50 m and 200 m. Observe that the algorithm prefers sonar depths close to the sound speed minimum (approximately 50 m depth). For these highly beneficial sound speed profiles, placement of the sonar within the channel will result in long-range detection of targets also within the channel, see Fig. 4. Placement close to the sound speed minimum also minimises the interaction with the surface, where the surface bubble layer and waves will attenuate and scatter the transmitted pulse.

The target's goal is two-fold; it wants to remain undetected while retaining its ability to detect surface targets. Fig. 4 shows the target depth distribution proposed by the algorithm, along with the averaged active sonar detection probability for $d = 50$ m on the left. The available target depths are bounded between 30 m depth and 30 m above the minimum bottom depth within each subarea, as indicated in the figure. Comparing the two figures side by side, it is clear that the target avoids the sound channel above 100 m. Outside this channel, the target generally prefers shallower depths, as the passive sonar range generally decreases with depth. This is shown in Fig. 5 along with the standard deviation of the active sonar detection. The latter plot also shows that the active detection performance can be quite variable beyond 10 km for depths between 100 m and 150 m, shown as a white-blue stripe.

The peak observed at 270 m in the target depth distributions may be attributed to the histogram of lower target depth bounds, as shown in Fig. 4. In 28% of the cases, the calculated Nash equilibrium has its maximum probability at the deepest allowed target depth. The target attempts to avoid detection by going as deep as possible, which therefore makes the strategy distribution toward the deep end mirror the distribution of the lower bound. The most prominent peak at 210 m, however, seems to indicate a hiding

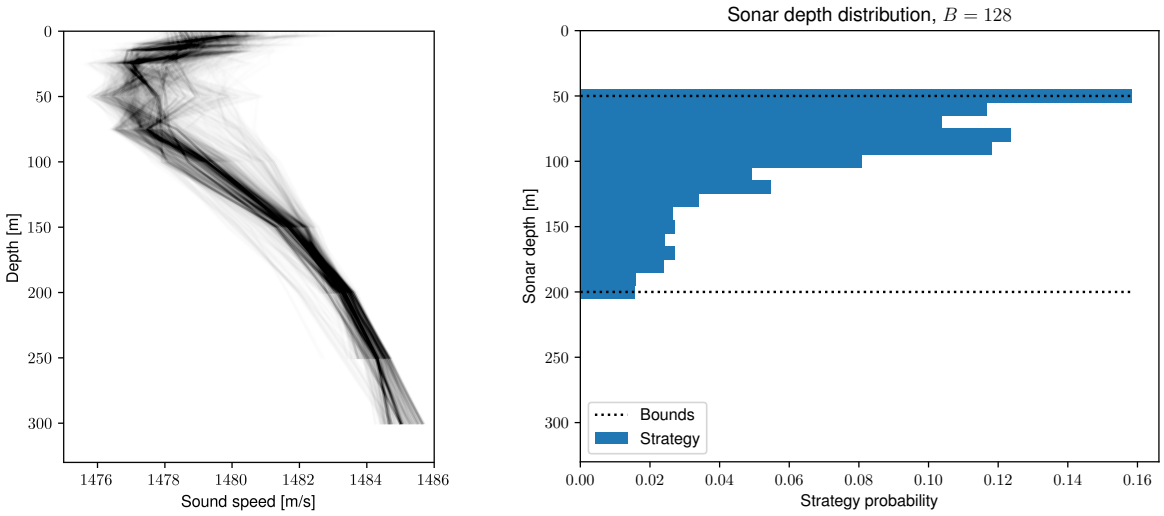

Figure 3: Left: Cloud of SSPs used in the modelling. The SSPs are derived from the NorKyst800 model described in section 3. Right: Distribution of resulting optimised sonar depths, d, based on the proposed method.

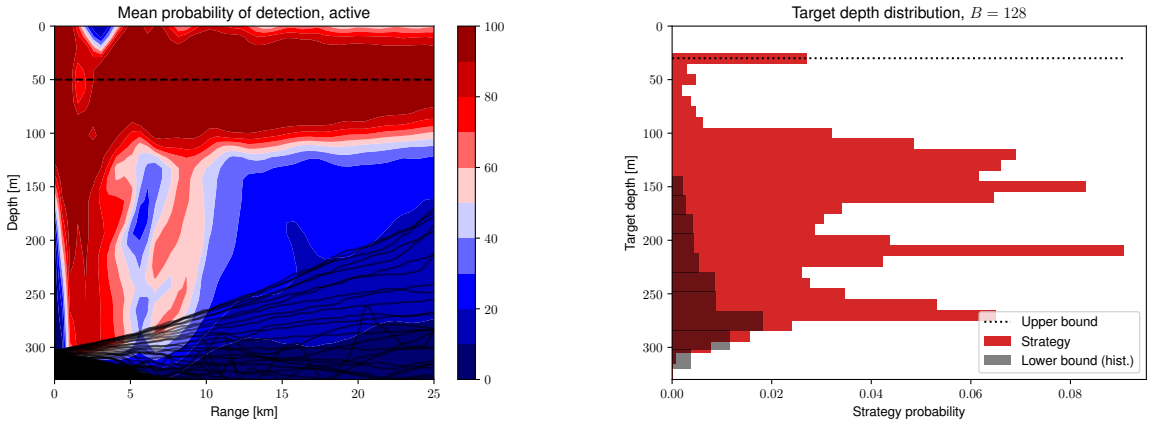

Figure 4: Left: Mean (over time and bearing) modelled probability of active sonar detection of the underwater target for the sonar depth with the highest strategy probability (indicated by a black, dashed line). The solid black lines are the bottom profiles for different bearings. Right: Distribution of resulting optimised target depths, z, based on the proposed method, along with histogram of lower bounds for each area (not to scale).

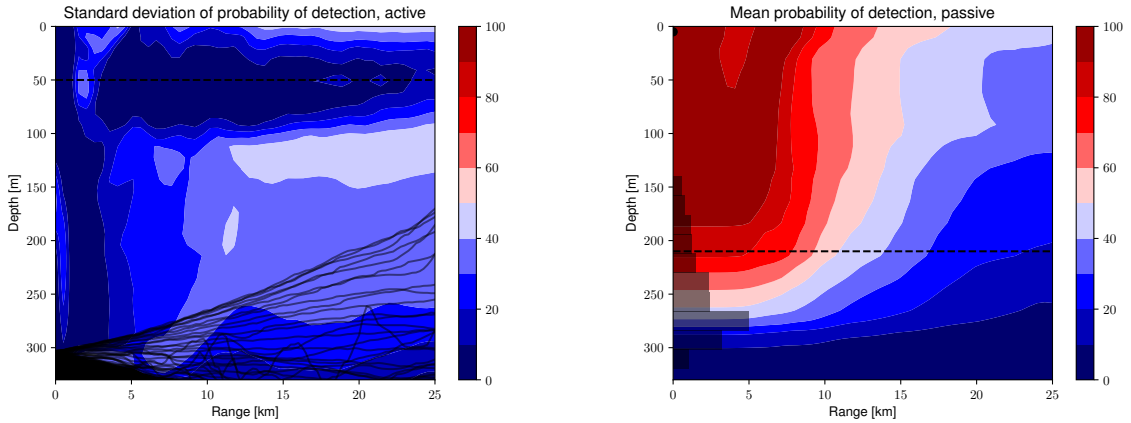

Figure 5: Left: Standard deviation (over time and bearing) of modelled probability of active sonar detection of the underwater target for the sonar depth with the highest strategy probability (indicated by a black, dashed line). The solid black lines are the bottom profiles for different bearings. Right: Mean (over time and position) modelled probability of passive sonar detection by the underwater target of a surface target. Histogram of lower bounds for each area also shown.

depth which is abnormally invariant of time, bearing and range. This may be partially due to peaks in the bottom reverberation levels hiding the target's echo, seen as the blue patch around 5 km in Fig. 4.

The strong spatial dependence in both topography and oceanography in this area requires a high number of subareas to achieve stable results. This is illustrated in Fig. 6. As the number of bearings used, B, increases, the depth distributions converge when considering the Euclidean distance in probability space from the $B = 128$ distributions:

$$\delta(\boldsymbol{R}_B^{\mathcal{Z}/\mathcal{D}}, \boldsymbol{R}_{128}^{\mathcal{Z}/\mathcal{D}}) = \sum_{z/d} (\boldsymbol{R}_B^{z/d} - \boldsymbol{R}_{128}^{z/d})^2 \tag{3}$$

The distributions for $B = 64$ fall within 1% of the distributions derived for $B = 128$. The number of bearings required for sufficiently accurate results will depend on both the spatial variability in the considered area and the requirements for accuracy. A difference of 1% is by this metric less than the difference between a fair coin and one with 51% odds for heads and 49% for tails.

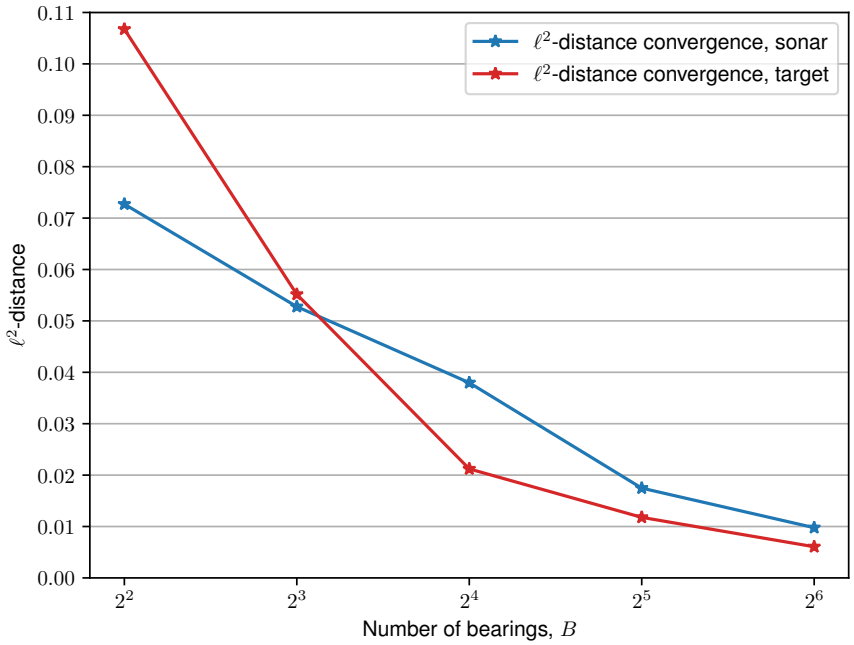

Figure 6: The ℓ^2-distance (Euclidian distance) of the distributions from those with $B = 2^7 = 128$ versus the number of bearings included in the method.

5 CONCLUSION

From the aggregated active sonar and target depth strategies shown in Fig. 3 and 4 we can conclude that there is no single best depth when you take variability into account. Previous work[7] showed that this was already the case for a single environmental realisation due to mixed strategies, but even these mixed strategies are not themselves stable. In this work, however, we see that certain trends in the strategies, like the peak at 210 m in Fig. 4, remain stable throughout the varying environment. The peaks also display spread in depths, akin to the Gaussian filter applied to single mixed strategies previously[7]. The strategies aggregated over environmental variability are therefore more robust against slight variations than those generated from a single realisation.

It should be remarked that the distribution created by aggregating the optimal strategies for each (t, θ, r) is not itself an optimal strategy for the whole area. This is most obvious when considering the target depth, as we see that e.g. the peak at 210 m in Fig. 3 is below the lower bound caused by the bottom depth in some subareas. Uncertainty in which subarea the target is located can be properly treated by defining a Bayesian game, where Bayesian-Nash equilibrium strategies constitute true optimal strategies[10]. If, however, the goal is to calculate expected sonar ranges integrated over likely target depths in an environment, or to use sensible sonar depths in Monte Carlo simulations, sampling from distributions like those in Fig. 3 and Fig. 4 can be sufficient. This would result in more accurate performance evaluations and less time wasted on strategically unreasonable simulations.

REFERENCES

1. E. M. Bøhler, K. T. Hjelmervik, and P. Østenstad, "A Monte Carlo approach for capturing the uncertainty in sonar performance modelling," in *Global Oceans 2020: Singapore – U.S. Gulf Coast*, pp. 1–8, Oct. 2020.
2. J. Albretsen, A. K. Sperrevik, A. Staalstrøm, A. D. Sandvik, F. Vikebø, and L. Asplin, "NorKyst-800 Report No. 1: User manual and technical descriptions," Tech. Rep. 2-2011, Institue of Marine Research, Feb. 2011.
3. K. Heaney and H. Cox, "A Tactical Approach to Environmental Uncertainty and Sensitivity," *IEEE Journal of Oceanic Engineering*, vol. 31, pp. 356–367, Apr. 2006.
4. K. R. James and D. R. Dowling, "A method for approximating acoustic-field-amplitude uncertainty caused by environmental uncertainties," *The Journal of the Acoustical Society of America*, vol. 124, pp. 1465–1476, Sept. 2008.
5. K. T. Hjelmervik and E. M. Bøhler, "Optimization of active sonar parameters in a measured environment," in *6th Underwater Acoustics Conference and Exhibition*, 2021. Place: Virtual Meeting.
6. F. B. Jensen, W. A. Kuperman, M. B. Porter, and H. Schmidt, "Ray Methods," in *Computational Ocean Acoustics* (F. B. Jensen, W. A. Kuperman, M. B. Porter, and H. Schmidt, eds.), Modern Acoustics and Signal Processing, pp. 155–232, New York, NY: Springer, 2011.
7. K. E. Andreassen and K. T. Hjelmervik, "Modelled sonar and target depth distributions for active sonar operations in realistic environments," *Proceedings of Meetings on Acoustics*, vol. 47, p. 070013, Sept. 2022.
8. J. F. Nash, "Equilibrium points in n-person games," *Proceedings of the National Academy of Sciences*, vol. 36, pp. 48–49, Jan. 1950.
9. E. Dombestein and T. Jenserud, "Improving Underwater Surveillance: LYBIN Sonar performance Prediction," in *MAST Americas 2010*, 2010. Place: Washington DC, USA.
10. N. Nisan, T. Roughgarden, E. Tardos, and V. V. Vazirani, eds., *Algorithmic Game Theory*. Cambridge: Cambridge University Press, 2007.
11. J. F. Nash, "Non-Cooperative Games," *Annals of Mathematics*, vol. 54, no. 2, pp. 286–295, 1951.
12. V. Knight and J. Campbell, "Nashpy: A Python library for the computation of Nash equilibria," *Journal of Open Source Software*, vol. 3, p. 904, Oct. 2018.
13. GEBCO Compilation Group, "GEBCO 2023 Grid," 2023.